



Ventral Pallidal GABAergic Neuron Calcium Activity Encodes Cue-Driven Reward Seeking and Persists in the Absence of Reward Delivery

Alexandra Scott,^{1,2} Dakota Palmer,^{1,2}  Bailey Newell,^{2,3} Iris Lin,^{2,3} Christelle A. Cayton,^{2,3} Anika Paulson,^{2,3} Paige Remde,^{2,3} and  Jocelyn M. Richard^{2,3}

¹Graduate Program in Neuroscience, University of Minnesota, Minneapolis, Minnesota 55455, ²Medical Discovery Team on Addiction, University of Minnesota, Minneapolis, Minnesota 55455, and ³Department of Neuroscience, University of Minnesota, Minneapolis, Minnesota 55455

Reward-seeking behavior is often initiated by environmental cues that signal reward availability. This is a necessary behavioral response; however, cue reactivity and reward-seeking behavior can become maladaptive. To better understand how cue-elicited reward seeking becomes maladaptive, it is important to understand the neural circuits involved in assigning appetitive value to rewarding cues and actions. Ventral pallidum (VP) neurons are known to contribute to cue-elicited reward-seeking behavior and have heterogeneous responses in a discriminative stimulus (DS) task. The VP neuronal subtypes and output pathways that encode distinct aspects of the DS task remain unknown. Here, we used an intersectional viral approach with fiber photometry to record bulk calcium activity in VP GABAergic (VP GABA) neurons in male and female rats as they learned and performed the DS task. We found that VP GABA neurons are excited by reward-predictive cues but not neutral cues and that this response develops over time. We also found that this cue-evoked response predicts reward-seeking behavior and that inhibiting this VP GABA activity during cue presentation decreases reward-seeking behavior. Additionally, we found increased VP GABA calcium activity at the time of expected reward delivery, which occurred even on trials when reward was omitted. Together, these findings suggest that VP GABA neurons encode reward expectation, and calcium activity in these neurons encodes the vigor of cue-elicited reward seeking.

Key words: calcium activity; cues; fiber photometry; motivation; reward; ventral pallidum

Significance Statement

VP circuitry is a major driver of cue-evoked behaviors. Previous work has found that VP neurons have heterogeneous responses and contributions to reward-seeking behavior. This functional heterogeneity is because of differences of neurochemical subtypes and projections of VP neurons. Understanding the heterogeneous responses among and within VP neuronal cell types is a necessary step in further understanding how cue-evoked behavior becomes maladaptive. Our work explores the canonical GABAergic VP neuron and how the calcium activity of these cells encodes components of cue-evoked reward seeking, including the vigor and persistence of reward seeking.

Received Jan. 3, 2023; revised June 1, 2023; accepted June 10, 2023.

Author contributions: A.S. and J.M.R. designed research; A.S., D.P., B.N., I.L., C.A.C., A.P., P.R., and J.M.R. performed research; A.S., D.P., B.N., C.A.C., and J.M.R. analyzed data; A.S. and J.M.R. wrote the paper.

This work was supported by National Institutes of Health—National Institute on Drug Abuse (NIH—NIDA) Grant R01DA053208 to J.M.R., NIH—NIDA Grant F31DA055442 to D.P., and a MnDRIVE Graduate Fellowship in Neuromodulation to A.S. Some viral vectors used in this study were generated by the University of Minnesota Viral Vector and Cloning Core.

The authors declare no competing financial interests.

Correspondence should be addressed to Jocelyn M. Richard at richardj@umn.edu or Alexandra Scott at scot0817@umn.edu.

<https://doi.org/10.1523/JNEUROSCI.0013-23.2023>

Copyright © 2023 the authors

Introduction

Environmental cues associated with rewards are powerful modulators of reward-seeking behavior. Understanding how environmental cues can invigorate reward-seeking behavior is a necessary step in learning how cue reactivity, and subsequent reward seeking, can become maladaptive. The ventral pallidum (VP) is a part of the ventral basal ganglia and an important node in the neural circuitry mediating cue-evoked reward-related behavior (Tindell et al., 2004, 2005; Smith et al., 2009; Richard et al., 2016, 2018; Ottenheimer et al., 2018; Lederman et al., 2021). VP neurons have heterogeneous responses to both rewards and cues predictive of rewards. Most VP neurons are excited by reward-predictive cues, whereas a smaller population is inhibited by the same cues.

Additionally, the firing rates of some cue-excited VP neurons can predict the vigor of reward seeking in response to that cue (Richard et al., 2016, 2018; Lederman et al., 2021). VP neurons are also sensitive to reward identity and prior reward history (Lederman et al., 2021). Whether the VP neurons encoding reward-predictive cues, reward-seeking vigor, and reward identity are the same or distinct subsets of VP neurons remains unknown. Therefore, exploring the neurochemical and projection-specific identity of VP neurons is an important step to understanding the broader neural circuitry that has an impact on reward-seeking behavior.

Recent research has begun to probe which VP neuronal cell types contribute to distinct aspects of reward processing and reward-seeking behavior (Kupchik and Prasad, 2021). The VP contains three major neuronal subtypes—cholinergic, glutamatergic, and GABA (Root et al., 2015). VP glutamatergic neurons constrain reward seeking and promote aversion-related behavior (Faget et al., 2018; Tooley et al., 2018; Stephenson-Jones et al., 2020). In contrast, VP GABAergic (VP GABA) neurons are excited by rewards and Pavlovian reward-paired cues (Heinsbroek et al., 2020; Stephenson-Jones et al., 2020). Activation of VP GABA neurons drives positive reinforcement as well as cued drug seeking and relapse (Faget et al., 2018; Heinsbroek et al., 2020; Prasad et al., 2020; Farrell et al., 2022). Inhibition of VP GABA neurons can induce place avoidance and dampen risky decision-making (Faget et al., 2018; Heinsbroek et al., 2020; Farrell et al., 2021). Yet, how VP GABA neurons develop responses to reward-predictive cues over time, or if their activity predicts the vigor of reward seeking, remains unknown.

Here, we examined whether the calcium activity of VP GABA neurons encodes cues predictive of reward availability and how this activity is related to subsequent reward-seeking behavior. Rats were trained in a discriminative stimulus (DS) task with liquid sucrose reward while we recorded population-level calcium activity of VP GABA neurons using fiber photometry. We found that VP GABA neurons develop a calcium response to reward-predictive cues as rats learn the DS task. VP GABA calcium activity was found to respond following the reward-predictive cue, following the action required to obtain reward, and during reward consumption. Calcium increases postcue, and operant action persisted even on trials where reward was omitted. Additionally, VP GABA cue-evoked calcium activity was shown to correlate with behavioral responses that measure the vigor of reward seeking. Finally, we tested the impact of optogenetic inhibition of VP GABA neurons during cue presentations and found that rats were slower and less likely to respond to cues predicting reward availability. These results suggest that VP GABA neurons encode environmental cues predictive of sucrose reward, and this cued calcium response predicts and contributes to the vigor of reward-seeking behavior.

Materials and Methods

Subjects

Male and female Long–Evans rats ($n = 37$; 17 male, 20 female; Envigo), weighing 250–400 g at arrival, were individually housed in a temperature- and humidity-controlled colony room on a 12 h light/dark cycle. Rats were food restricted starting 3 d before the initiation of training in the DS task and until experiments were completed. Rats received 5% of their body weight in food each day, and the amount of food was adjusted daily to maintain rats at ~90% of their free-feeding body weight. All experimental procedures were approved by the Institutional Animal Care and Use Committee at the University of Minnesota and were conducted

in accordance with the *Guide for the Care and Use of Laboratory Animals* of the National Institutes of Health.

Surgeries

During surgery, rats were anesthetized with isoflurane (5%) and placed in a stereotaxic apparatus, after which surgical anesthesia was maintained with isoflurane (0.5–2.0%). Rats received preoperative injections of carprofen (5 mg/kg) for analgesia and cefazolin (75 mg/kg) to prevent infection. To achieve cell-type-specific calcium indicator expression we used a dual viral approach combining a glutamate decarboxylase 1 (GAD1) promoter virus for the expression of Cre recombinase with viruses for the expression of GCaMP6f, opsins, or control fluorophores in a cre-dependent manner (Liu et al., 2013; Wakabayashi et al., 2019; Shields et al., 2021). Syringes for viral delivery and optical fiber implants were aimed at the VP using the following coordinates relative to bregma: +0.3 mm anteroposterior (AP), ± 2.3 mm mediolateral (ML), -8.3 mm dorsoventral (DV). Rats intended for fiber photometry recordings or RNAscope analysis ($n = 19$; 9 male, 10 female) received a mixture of adeno-associated virus (AAV)9-Syn-Flex-GCaMP6f (1.05×10^{13} GC/ml final titer; Addgene) and AAV8-GAD1-cre (4.15×10^{13} GC/ml final titer; University of Minnesota Viral Vector Core) injected unilaterally into VP at a volume of $0.8 \mu\text{l}$. A subset of these rats ($n = 4$; 2 male, 2 female) also received, contralateral to the primary recording location, an infusion of AAV9-Syn-Flex-GCaMP6f and fiber implant into VP and a retrograde AAV8-GAD1-cre (AVVrg-GAD1-Cre; 1.03×10^{14} GC/ml; University of Minnesota Viral Vector Core) into lateral hypothalamus (-2.9 mm AP, 1.8 mm ML, -8.4 mm DV). This combination of injections did not lead to GCaMP6f expression. Thus, these recordings are included in the no expression control dataset. For external controls ($n = 2$; 2 female) $0.8 \mu\text{l}$ of a mixture of EGFP (AAV9-Syn-DIO-EGFP; 2.3×10^{13} GC/ml final titer; Addgene) and AAV8-GAD1-cre was injected unilaterally into VP. For experiments examining optogenetic inhibition of VP GABA neurons, rats received bilateral $0.4 \mu\text{l}$ injections of a mixture of AAV8-GAD1-Cre (1.03×10^{12} GC/ml final titer) mixed with either AAV1-Syn-SIO-stGtACR2-FusionRed ($n = 10$; 5 male, 5 female; 4.17×10^{11} GC/ml final titer) for optical inhibition or AAV8-Syn-DIO-mCherry ($n = 6$; 3 male, 3 female; 2.0×10^{12} GC/ml final titer) as a control group.

Virus was delivered through 28 gauge injectors at a rate of $0.1 \mu\text{l}$ per min. Injectors were left in place for 10 min following the infusion to allow the virus to diffuse away from the infusion site. Following viral injections, rats used for fiber photometry measurements and optogenetic testing ($n = 31$; 14 male, 17 female) received fiber implants (0.48 NA, $400 \mu\text{m}$, Doric Lenses for fiber photometry; 0.29 NA, $300 \mu\text{m}$, RWD Life Science for optogenetics) in VP for optical measurement and manipulation of activity. Implants were secured to the skull with bone screws and dental acrylic. Rats recovered for at least 1 week before beginning handling. To allow for sufficient viral expression, rats recovered for at least 4 weeks before fiber photometry measurements, optogenetic manipulations, or brain extractions for RNAscope.

Discriminative stimulus task

Rats were trained in a discriminative stimulus (DS) task as described previously (Ottenheimer et al., 2018; Richard et al., 2018; Gómez-A et al., 2022). The DS task is an instrumental task where rats learn to discriminate between reward-predictive (DS) and neutral stimulus (NS) cues. Auditory cues consisted of a siren or white noise, with cue assignments counterbalanced across subjects. Rats received reward if they entered the port during the DS cue but not the NS cue. Over time, rats learn to discriminate between the cues, responding almost exclusively to the DS. Fiber photometry rats were tethered throughout training to measure GCaMP6f fluorescence, whereas optogenetic rats were tethered during the final training phase before testing.

Initial training (port training and Stages 1–4). Before training with cues, rats underwent port training in the operant boxes. In port training sessions, animals received 30 trials of 10% sucrose delivery. For each trial, once sucrose reward was retrieved from the port, another trial was initiated. Once rats met the criteria of 30 reward retrievals in 1 h, they transitioned to Stage 1 of DS task training. In Stages 1–4 of the DS task,

each session consisted of 30 DS trials. Each trial consisted of a window in which an auditory cue (DS; siren or white noise) signaled 10% sucrose availability for up to 60 s (Stage 1), 30 s (Stage 2), 20 s (Stage 3), or 10 s (Stage 4). The DS cue played until the rat entered the port or the availability window was over. Intertrial intervals (ITI) were pseudorandom and adjusted so that the average time between the start of each DS presentation was 120 s (i.e., as the DS length decreased, the ITI lengthened from 60 to 110 s). Fiber photometry rats were required to respond during at least 70% of DS presentations (0.70 response probability) to pass each stage. After meeting these criteria for Stage 4, rats moved on to the full version of the DS task. Rats trained for optogenetic manipulations were required to respond to at least 60% of DS presentations before moving on to the next phase. Rats that reached Stage 4 criteria paused training until the remaining rats met criteria, and then all rats completed 3–4 additional days of Stage 4 training.

Full DS task training (Stage 5). The full version of the DS task (Stage 5) consisted of 60 trials, 30 of which were DS and 30 of which were NS. The DS was presented for a maximum of 10 s, or until the animal entered the port. The NS played for 10 s independent of animal behavior. DS or NS trial order was determined pseudorandomly. Intertrial intervals were determined pseudorandomly with an average interval time of 50 s (30–70 s). A criterion of 0.70 DS response probability and 0.30 NS response probability was required for fiber photometry animals to complete Stage 5. Rats tested for the effects of optogenetic inhibition were trained to these criteria or until their DS response probability was at least 50% greater than their NS response probability.

Probe trials and extinction. Following completion of Stage 5 testing in the fiber photometry rats, we added a 1 s delay between the port entry and reward delivery, as well as probe trials for 50% of DS presentations. During probe trials, port entries during the DS were not followed by reward delivery. This allowed us to better determine whether we saw distinct calcium responses to the cue presentation, port entry, and initial lick bouts. Rats underwent 2 d of testing under these conditions. Finally, animals underwent 3 d of extinction in which sucrose was no longer delivered.

In vivo calcium recordings

Fiber photometry recordings were done throughout training in the DS task. Recordings were conducted according to methods described previously (Saunders et al., 2018). Rats were first acclimated to the tethering cable (0.48, 400 μm core optical fiber) and the operant box. During recording sessions, the tethering optical fiber is connected to a fluorescent mini cube (Doric Lenses), which transmits excitation light from both a 465 nm LED and a 405 nm LED. The 465 nm excitation stimulates calcium-dependent GCaMP6f fluorescence, and the 405 nm excitation stimulates GCaMP6f fluorescence in a calcium-independent fashion. GCaMP6f fluorescence travels to the minicube via the tethering cable, passes through a GFP emission filter, and is amplified and focused onto a high sensitivity photodetector. A real-time signal processor (RZ5P, Tucker-Davis Technologies) running Synapse software was used to modulate the output of each LED and record photometry signals. Before each session, the power level for each LED was measured and adjusted to a range of ~ 10 –25 microwatts (Meng et al., 2018). The offset for each animal was kept constant, between 20–30 mA (Tucker-Davis Technologies user manual), and the level was adjusted to obtain the appropriate power. The 465 nm LED driver frequency was set to 211 Hz, and the 405 nm LED driver frequency was set to 531 Hz. This allowed for demodulation of the separate LED signals, yielding a calcium-dependent signal and a calcium-independent signal (isosbestic signal; Tian et al., 2009; Dana et al., 2018; Patel et al., 2019) to use as an internal control for each animal. Task events (cue presentations, port entries, and lick bouts) were time stamped in the photometry data file via a transistor-transistor logic (TTL) signal generated by the behavioral equipment (Med Associates SuperPort and TTL panel). Video recordings were simultaneously collected from each operant box (Amcrest).

Calcium-dependent fluorescent changes were detected in the calcium-dependent channel (465 nm), whereas calcium-independent fluorescent changes were detected in both the dependent and independent

(405 nm, isosbestic) calcium channels. VP GABA bulk activity is represented as a change in fluorescence over time. Calcium-dependent and independent channels were fit and combined to control for any artifacts not associated with neuronal activity. This combined signal ($\Delta F/F$) was normalized in perievent time windows for each trial, where baseline activity 5 s before cue presentation was used to calculate a z score for each $\Delta F/F$ data point in the perievent window.

Optogenetic manipulations

Rats were tested after reaching behavioral criteria in the DS task while tethered to optical patch cables (200 μm core, 0.4 m split cables, Doric Lenses), connected to a rotary join on a cantilever arm, which was connected to a 473 nm laser (DPSS Lasers). On test days, rats received continuous photoillumination of the VP (10–15 mW light power) on 50% of DS and NS trials, pseudorandomly selected. Photoillumination was initiated at the start of the cue and terminated after 1 s on test day 1 and after port entry or the end of the DS (whichever occurred first) on test day 2. Control virus rats received additional test days with 1 s of 20 Hz or 40 Hz photoillumination, which are not reported here.

Behavioral analysis

DS and NS response probabilities were calculated for each cue type as the ratio between the number of trials where the animal entered the port within 10 s of cue onset to the number of overall trials for each specific cue type. We used port entry latency as a behavioral proxy for reward-seeking vigor and motivation (Richard et al., 2018; Lederman et al., 2021). Port entry latency was calculated as the difference between port entry time points and cue onset time points. Port entry latency was only calculated on trials where animals entered the port within 10 s of cue presentation, allowing for a more consistent measure of latency across stages. One animal was excluded from fiber photometry analyses for lack of cue discrimination after 12 d of Stage 5 training. To examine how the port entry probability developed across training, two linear mixed-effects models were run. For training sessions between Stages 1 and 4, the model was fit with fixed effects for day and sex, and a random effect of subject. For Stage 5 sessions, the model was fit with fixed effects for day, sex, and cue type, and a random effect of subject. To assess final performance in fiber photometry rats, a paired t test was run for criteria day port entry probability and latency between cue types. To assess the impact of optogenetic inhibition, we fit linear mixed-effects models for port entry latency and probability, with a random effect for subject, and fixed effects for trial type (DS vs NS, laser vs no laser), viral group and/or laser duration, as appropriate.

Fiber photometry analysis

Postcue response across training. Fluorescent values and behavioral time stamps were exported to MATLAB software. Each training session was analyzed in a custom MATLAB script (available on request). Signals driven by 465 nm and 405 nm LEDs were downsampled to 40 Hz, fit to one another, and combined ($(465 \text{ nm} - \text{fitted } 405 \text{ nm})/\text{fitted } 405 \text{ nm}$; $\Delta F/F$) to control for any artifacts not associated with neuronal activity. Z -scores of the $\Delta F/F$ photometry signals for each trial were calculated based on the mean and SD of fluorescent values 5 s before the cue. We used an area under the curve (AUC) analysis on z -scored trial traces to collect a single value between 0 and 5 s postcue (when the bulk of the DS calcium event occurred) to run linear mixed-effects models. To examine how the calcium signal developed across training, two linear mixed-effects models were run. For training sessions between Stages 1 and 4, the model was fit with fixed effects for day and sex, and a random effect of subject. For Stage 5 sessions, the model was fit with fixed effects for day, sex, and cue type and random effect of subject. Depending on the best-fitting covariance model (Verbeke, 1997), the degrees of freedom may be a noninteger value. Any significant interactions were further assessed with pairwise comparisons with Sidak corrections for multiple comparisons. Because we did not observe any significant effects of sex, or interactions of sex and other factors (F values ranging from 0.051 to 1.37) we report data pooled across males and females for these analyses.

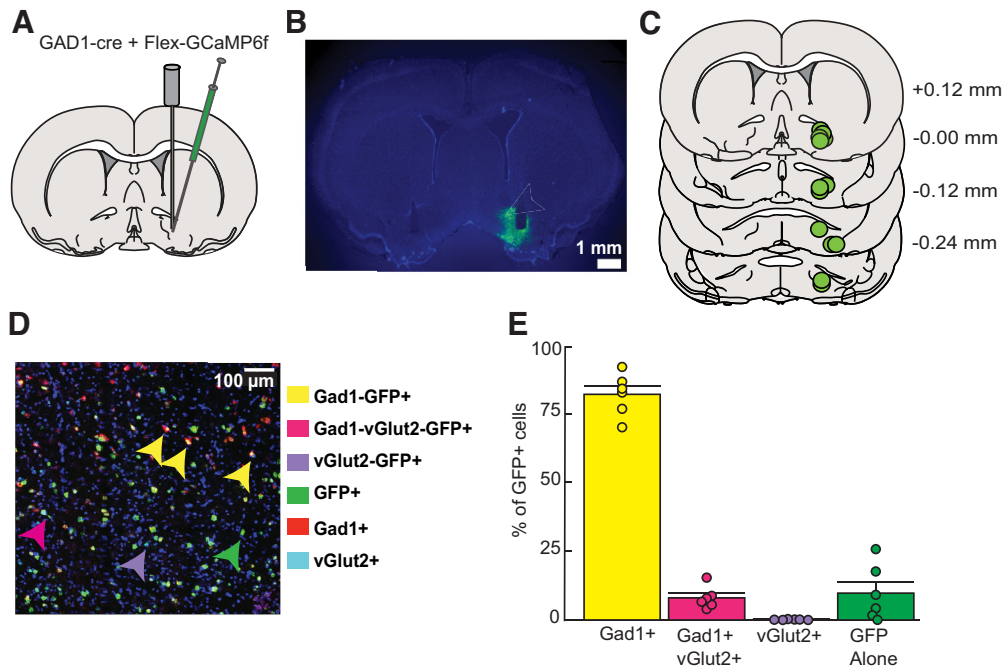


Figure 1. Anatomical and cellular characterization of GCaMP6f expression in VP. **A**, Diagram of intersectional viral approach and fiber optic implant used for cell-type-specific calcium recordings in the VP. **B**, Representative image of virally expressed GCaMP6f and optical fiber tract placement in VP for calcium activity recordings (right) and for no-expression control recordings (left). **C**, Verification of fiber and expression at calcium activity recording sites in VP-containing coronal sections. Values listed indicate distance (millimeters) from bregma. **D**, Representative image of RNAscope processed tissue with arrows denoting location of each defined GCaMP6f-expressing (GFP+) cell type. **E**, Quantification of the percentage of GFP+ cells expressing Gad1, vGlut2, or both cell-type-specific markers, $n = 6$; three VP sections used for each subject's average ($82.09 \pm 3.14\%$ Gad1, $0.12 \pm 0.05\%$ of glutamatergic, $8.03 \pm 1.63\%$ Gad1/Vglut2/GFP, $9.75 \pm 4.12\%$ of just GFP+). Data are mean \pm SEM. Dots represent individual rats.

Isolating postcue responses to behavioral events. To isolate calcium signals associated with the cue from that of the port entry and reward delivery, we ran an encoding model on Z-scored calcium perievent time windows (Parker et al., 2016). The analysis isolates each time stamped event (cue presentation, port entry, initial lick onset) and relates that to each sampling point recorded from the calcium signal. To do this, event onset time stamps were transformed into binary indicators for each sampling point. Then, linear regression was run using the z-scored, Stage 5 GCaMP6f recordings as the response variable and the transformation of the time stamps of the cue presentation, port entry, and initial licks as the predictor variables. This regression model output provided response kernels for each distinct event. AUC values were then acquired from regression kernels, and Student's *t* tests were run defining the significance of the AUC from null.

Postcue correlation to reward-seeking motivation. To determine whether DS-evoked neuronal activity predicts the latency of reward seeking, our behavioral proxy of reward-seeking motivation, we ran a linear correlation analysis relating the peri-DS Z-scored delta F/F calcium signal from Stage 5 trials to trial-by-trial port entry latency (Pearson's correlation coefficients) for each rat. Because the encoding model described above revealed significant port-entry-related increases in calcium activity after, but not before, port entry, for our correlation analysis we excluded fluorescence recorded from any post-port-entry time points. We also shuffled these data to create random control data for comparison to the true calcium and latency relations. Comparison of the shuffled and unshuffled correlations were done in 0.10 s time bins with multiple *t* tests with Sidak corrections for multiple comparisons.

Histology

Validation of fiber placement and region-specific expression. Following completion of behavioral testing with fiber photometry recordings and optogenetic manipulations, animals ($n = 31$; 14 male, 17 female) were deeply anesthetized with pentobarbital and were

perfused intracardially with 0.9% saline followed by 4% paraformaldehyde. Brains were removed, postfixed in 4% paraformaldehyde for 4–24 h., cryoprotected in 30% sucrose for >48 h, and sectioned at $40 \mu\text{m}$ on a microtome. Sections were then washed with PBS, wet mounted on coated glass slides in PBS, air dried, coverslipped with VECTASHIELD mounting medium with DAPI, and imaged on a fluorescent microscope. We verified the location of injection or optical fiber recording sites using anatomic markers of VP (anterior commissure, lateral ventricle size). We excluded two rats (female, *stGtACR2*) from the optogenetic manipulation experiments based on fiber misplacement and insufficient viral expression. Additionally, fiber implants in the contralateral VP were originally implanted in a subset of fiber photometry subjects to record from lateral hypothalamus projecting VP GABA neurons; however, viral expression was not obtained, and no fluorescent protein was expressed in the cells. We used recordings from these animals ($n = 4$; 2 male, 2 female) as no expression control sessions. Placement of fiber was assessed for these control recordings as well and confirmed to fall within VP.

Validation of cell-type-specific GCaMP6f expression. Animals designated for RNAscope analysis ($n = 6$; 3 female, 3 male) were deeply anesthetized with pentobarbital and decapitated. Fresh tissue was extracted and flash frozen in dry-ice-cooled isopentane. Brains were stored in a -80°C freezer for up to 1 year. Tissue was stored until sectioning of tissue was done on the cryostat (coronal sections, $16 \mu\text{m}$) and jump mounted for RNAscope processing. Tissue was processed to determine the location and extent of viral expression and neural identity of the neurons recorded. To validate our viral approach, we used RNAscope *in situ* hybridization with probes for *Gad1*, *Slc17a6* (*Vglut2*) and *GCaMP6* (Fig. 1D,E). The channels were, respectively, GCaMP6 probe (488 nm excitation), glutamatergic probe (*Slc17a6*, 555 nm excitation), and GABAergic probe (*Gad1*, 647 nm excitation). Imaging of the tissue was done on a confocal (Nikon upright C2, University Imaging Centers, University of Minnesota) at $20\times$ with $2\times$ digital zoom, and settings were optimized with the help of the University Imaging Centers at the University of Minnesota. The exact same acquisition settings were used on all tissue

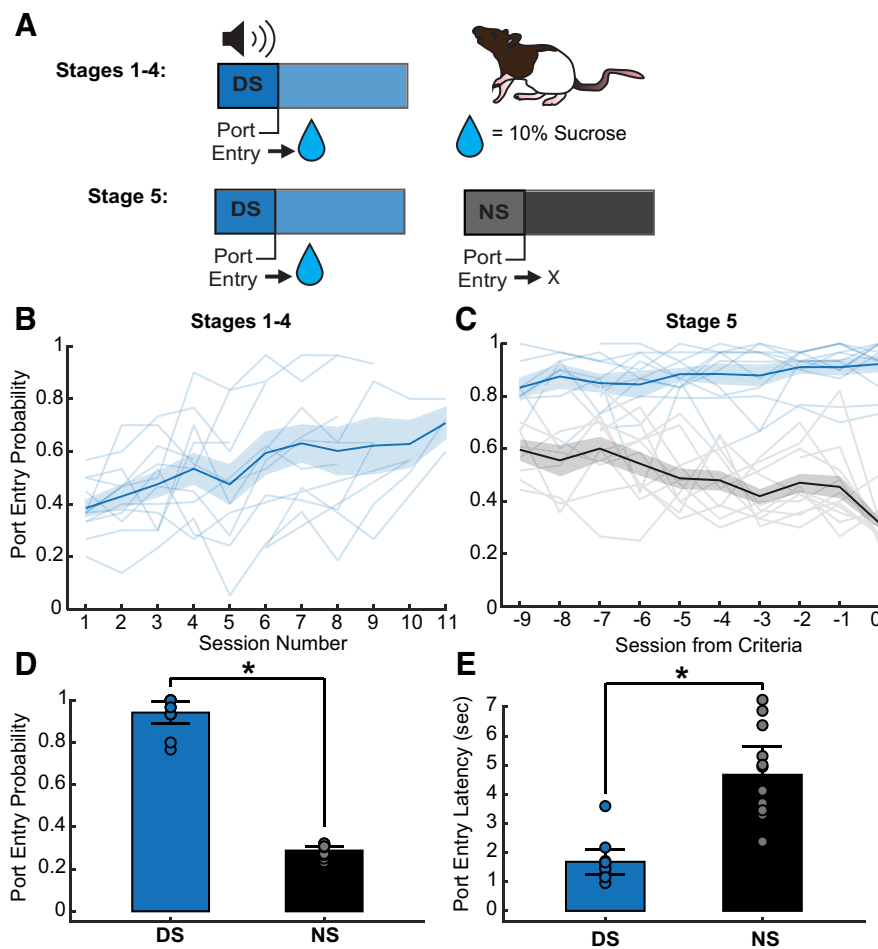


Figure 2. Behavioral task and training data. **A**, DS behavioral task trial design using 10% sucrose reward. **B**, DS response probability (blue) during Stages 1–4 of DS task (session effect, $F_{(1,98.36)} = 93.01, p < 0.001$). The line with shading indicates mean \pm SEM. Lines alone indicate individual subjects. **C**, Average DS (blue) and NS (black) response probability across the last 10 d of Stage 5 training (9 d before criteria is reached; session by cue effect, $F_{(1218,46)} = 25.32, p < 0.001$). The line with shading indicates mean \pm SEM. Lines alone indicate individual subjects. **D**, Average DS and NS response probability on the day discrimination criteria was reached (paired *t* test, $*p < 0.001$). Data are mean \pm SEM. Dots represent individual rats. **E**, Average DS and NS port entry latency on day discrimination criteria reached (paired *t* test, $*p < 0.001$). Data are mean \pm SEM. Dots represent individual rats.

samples. HALO software (Indica Labs) quantified the amount of cell specificity achieved from viral injections (He et al., 2020; McMillan et al., 2020; Buck et al., 2021; Fries-Craft et al., 2021; Giannini et al., 2021; Shahidehpour et al., 2021). Briefly, total cell number and location within an image was determined by nuclear staining (DAPI). Probes (Gad1, vGluT, GCaMP6) are assigned their respective fluorophores within the software, and the software compares the location of each fluorophore to the location of the DAPI-labeled cells to confirm fluorophore expression is associated with a self-defined nuclei and cell size. HALO analysis software and software settings were optimized for the tissue from all animals, and then settings were used to batch analyze cell counts of GCaMP6f-positive cells. No difference was seen in expression between different subregions of VP. The percentage and number of each defined cell identity of interest were determined for three sections per animal to determine cell specificity within and between all subjects.

Results

Viral mixture and fiber implantation specifically targets ventral pallidal GABAergic neurons

A mixture of DIO-GCaMP6f and GAD1-Cre viruses were infused into VP to express the genetically encoded calcium

indicator (GCaMP6f) specifically in VP GABA neurons. For measurement of calcium-related fluorescence, an optical fiber was implanted into VP (Fig. 1A,B). All rats that underwent calcium activity recording had viral expression and fiber placements within VP (Fig. 1C). To validate the cell-type specificity of our viral approach, we used RNAScope *in situ* hybridization with probes for *Gad1*, *Slc17a6* (*Vglut2*) and GCaMP in rats that did not receive fiber implants (Fig. 1D). Because no difference was seen in expression or selectively in different subregions of VP, these data were pooled for analysis. Overall, GCaMP6f (GFP+) and *Gad1*-positive cells made up 90.12% of GFP+ cells ($82.09 \pm 3.14\%$ *Gad1*/GFP; $8.03 \pm 1.63\%$ *Gad1*/*Vglut2*/GFP; Fig. 1E). Therefore, the cells we were recording with fiber photometry during the DS task were primarily and selectively GABAergic. In contrast, only $0.12 \pm 0.05\%$ of GFP+ cells were exclusively glutamatergic. Finally, $9.75 \pm 4.12\%$ of cells were GFP+ with no glutamatergic or GABAergic probe expression.

Rats discriminate between reward-predictive and neutral cues

Rats ($n = 12$; 6 male, 6 female) were trained on an operant discriminative stimulus task where reward availability was signaled by a reward-predictive cue (DS). Rats received a 10% sucrose reward if they entered the operant chamber port (port entry) during DS presentations, but not if they entered during the control cue (NS) or noncue periods (Fig. 2A). During Stages 1–4 (DS alone) of the task, rats received presentations of just the DS, which decreased in length over sessions from 60 to 10 s incrementally. As expected, port entry probability during the DS increased significantly across sessions during this phase of training (Fig. 2B; session effect, $F_{(1,98.36)} = 93.01, p < 0.001$).

Once rats entered the port during at least 70% of DS presentations in Stage 4, they progressed to the full version of the task (Stage 5) in which the NS control cue was introduced (Fig. 2A). Rats were deemed capable of discriminating between the DS and NS when they met criteria of a minimum of 70% DS response probability and a maximum of 30% NS response probability. One animal was excluded for lack of cue discrimination after 12 d of Stage 5 training.

As expected, rats learned to discriminate between the DS and NS cues over time (Fig. 2C; interaction of session and cue, $F_{(1,218.46)} = 25.32, p < 0.001$), increasing their probability of entering the port during the DS, and decreasing their probability of entering the port during the NS. In addition to responding more frequently to the DS than the NS when they met criteria (Fig. 2D; $p < 0.001$), rats also entered the port more quickly following the DS compared with the NS on trials when they made a port entry (Fig. 2E; $p < 0.001$).

Ventral pallidal GABA neurons develop a calcium response following the onset of the reward-predictive cue but not the neutral cue

Fiber photometry measurements of calcium activity were conducted throughout training to assess the development of responses across learning of the DS task. Using these methods, as rats learned the task, we observed VP GABA neurons develop a calcium response following the onset of the DS (Fig. 3A) but not the NS (Fig. 3B). The VP GABA neuronal calcium response is not apparent in response to the DS during the first session of training (Fig. 3C). The AUC was calculated for the average Z-scored calcium trace of each individual rat during each session of training. For initial training with just the DS, we observed a significant effect of training session on the average AUC before the introduction of the NS (Fig. 3F; main effect of session, $F_{(8,63.53)} = 5.16$, $p < 0.001$). By the first day of Stage 5, when the NS is introduced, an increase in calcium activity occurs soon after DS onset and persists for nearly 10 s (Fig. 3D, blue line). Cue-evoked calcium activity in response to the NS is reduced relative to the DS (Fig. 3D, black line). On the day subjects met behavioral criteria for cue discrimination (70% or greater response to the DS, 30% or less for the NS) the VP GABA calcium response post-DS is robust and persists for closer to 5 s, whereas the post-NS response is minimal in amplitude and duration. AUC analysis for the last 10 sessions of Stage 5 training shows a significant difference between DS and NS calcium responses (Fig. 3G; main effect of cue, $F_{(1,194.18)} = 46.64$, $p < 0.001$). No effect of cue was seen in control recordings (GFP and no-expression controls; main effect of cue, $F_{(1,48.09)} = 0.20$, $p = 0.66$; main effect of control type, $F_{(1,10.99)} = 1.20$, $p = 0.30$; cue and control type interaction, $F_{(1,48.10)} = 0.66$, $p = 0.80$). These findings suggest VP GABA neurons develop a response to reward-predictive cues while learning the DS task but do not respond to neutral cues never paired with reward.

VP GABA neuronal response post-reward-predictive cue is associated with cue onset, operant behavior, and initial reward consumption

Prior work from electrophysiological recordings in VP has found that DS-excited single units increase their firing at a median time of 90 ms after cue onset and return to baseline within 1 s, even for units with the longest-duration responses (Richard et al., 2016, 2018). In contrast, we observed changes in fluorescence from population-level calcium activity in VP GABA neurons, starting ~ 1 s after cue onset and persisting in the average traces for multiple seconds. Although GCaMP6f is a fast calcium indicator (Chen et al., 2013), in terms of both rise and decay kinetics,

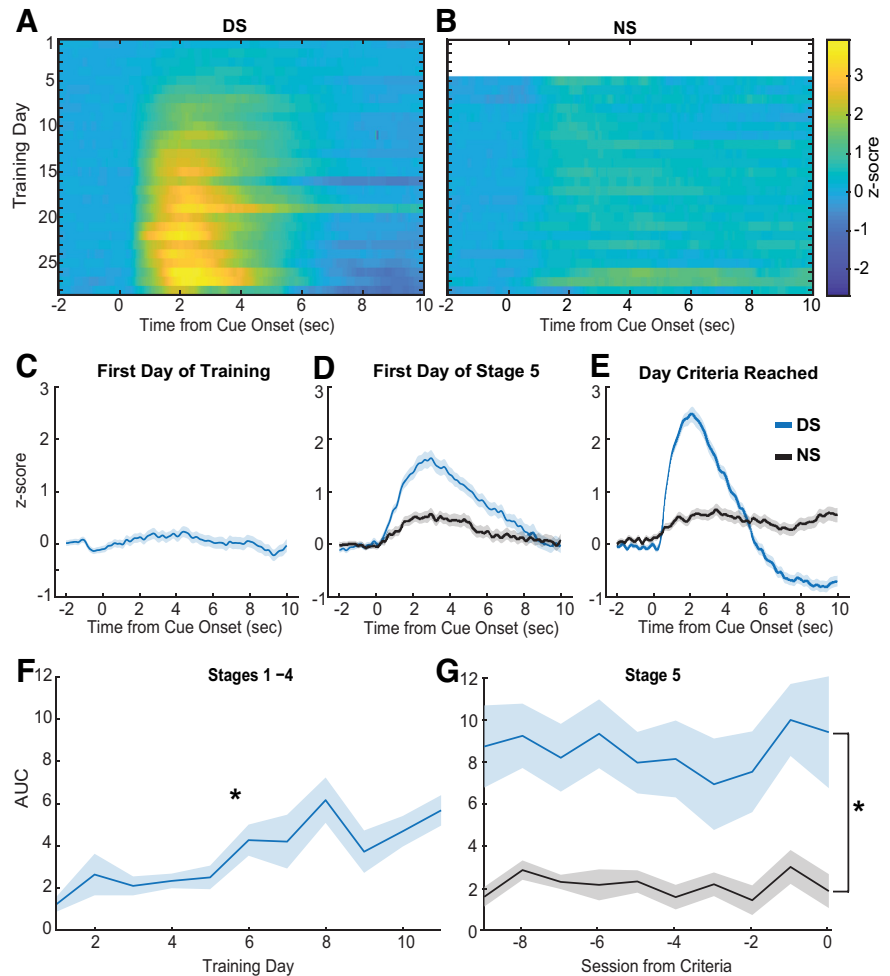


Figure 3. Calcium activity during training. **A**, Heat map of average Z-scored delta F/F response from VP GCaMP6f during the peri-DS cue time window (x -axis) across training days (y -axis) of all stages ($n = 12$ rats). **B**, Heat map of z-scored delta F/F response during the peri-NS cue time window across all Stage 5 training days ($n = 12$ rats). **C**, Average peri-DS calcium trace on day 1 of training ($n = 12$ rats; \pm SEM). **D**, Average pericue (DS, blue; NS, black) calcium trace on the first day of Stage 5 ($n = 12$ rats; \pm SEM). **E**, Average pericue calcium trace on the day each animal met criteria ($n = 12$; \pm SEM). **F**, Average AUC (0–5 s) of post-DS calcium traces across animals ($n = 12$; \pm SEM) during Stages 1–4 (main effect of session, effect, $F_{(8,63.53)} = 5.16$, $*p < 0.001$). **G**, Average AUC (0–5 s) of postcue calcium traces for the DS (blue) and NS (black) across animals ($n = 12$; \pm SEM) during the last 10 d of Stage 5 training (main effect of cue, $F_{(1,194.18)} = 46.6437$, $*p < 0.001$).

it still introduces slower dynamics compared with electrophysiological recordings (Wei et al., 2020). Prior work from electrophysiological recordings in the DS task has also found that VP single units are responsive to reward-seeking actions and at the time of reward consumption (Richard et al., 2016, 2018), and may encode the relative value of primary rewards or reward-prediction errors (Ottenheimer et al., 2018, 2020a,b) in addition to the incentive motivational value of cues. Therefore, it is likely that the calcium activity of VP GABA neurons is sensitive to multiple behavioral epochs following cue onset. That is, multiple calcium responses may contribute to the prolonged calcium trace seen when trials are averaged. When we sorted individual trials by the latency of the animals to enter the port, we observed both increased fluorescence that was time locked to the cue, as well as an increase that appeared to be time locked to the port entry after the DS presentation (Fig. 4A). We observed a similar pattern when we plotted the trials time locked to port entry and sorted by port entry latency (Fig. 4B). Moreover, when trials that were time locked to initial lick responses were sorted by port entry

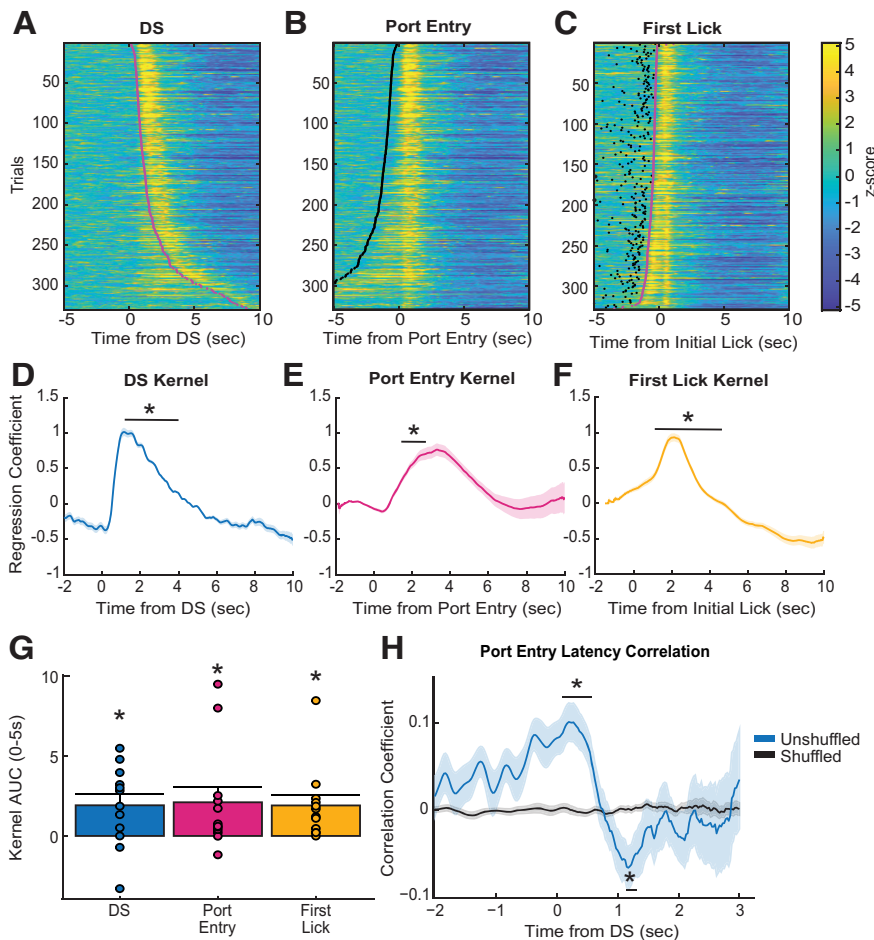


Figure 4. Event-related responses during performance of the DS task. **A**, Heat map of Z-scored responses from Stage 5 of a representative animal, trials sorted by port entry latency, time locked to the DS cue onset. Magenta dots represent the time of port entry. **B**, Heat map of Z-scored responses from Stage 5 of a representative animal, trials sorted by port entry latency, time locked to port entry. Black dots represent cue onset. **C**, Heat map of Z-scored responses from Stage 5 of a representative animal, sorted by port entry latency, time locked to initial lick onset. **D**, Average DS cue onset kernel of lasso regression coefficients across all animals ($n = 12$), significant difference from zero between 0.90 and 3.40 s time bins (*all p values < 0.05). **E**, Average port entry onset kernel of lasso regression coefficients across all animals ($n = 12$), significant difference from zero between 1.40 and 2.40 s time bins (*all p values < 0.05). **F**, Average initial lick onset kernel of lasso regression coefficients across all animals ($n = 12$), significant difference from zero between 1.30 and 3.60 s time bins (*all p values < 0.05). **G**, Average AUC of each regression kernel across animals ($n = 12$), t test comparing each AUC to zero. Mean + SEM, dots indicate individual subjects. **H**, Linear Pearson's correlation coefficients for trial latency of the animal to DS-evoked VP GABA calcium activity correlation (unshuffled, blue; shuffled, black). Time bin analysis indicated that true (unshuffled) coefficients were significantly different from zero between 0.00 and 0.50 s time bins (* $p < 0.006$), and 1.10 and 1.20 s time bins (* $p < 0.03$). Lines with shading indicate mean \pm SEM.

latency, we observed a distinct calcium response that occurs after initial lick onset, at least on trials where latency between reward delivery (time of port entry) and licking behavior is longer (Fig. 4C). Therefore, the extended calcium responses we see following DS onset could be related to all three behavioral epochs—sensing the cue, the operant action, and the initial reward consumption.

To test this, we ran an encoding model on the preveriet calcium data for each rat, for each trial, on the day the animal reached final behavioral criteria in Stage 5 of the DS task. This encoding model was adapted from Parker et al. (2016). Here, a binary of each behavioral epoch was correlated to each time point of the calcium signal, and separate kernels of regression coefficients were acquired for each behavioral epoch (Fig. 4D–F). A time bin analysis was run on each kernel, comparing the average kernel value at each 0.1 s time bin postevent onset to a null value, corrected for multiple comparisons. This analysis found

that the DS kernel was significantly greater than zero during 0.90–3.0 s time bins postcue (Fig. 4D; all p values < 0.05), the port entry kernel was significantly greater than zero during 1.40–2.40 s time bins (Fig. 4E; all p values < 0.05), and the initial lick kernel was significantly increased during 1.30–3.60 s time bins (Fig. 4F; all p values < 0.05). AUC analysis of the average kernels for each event indicated each kernel is significantly greater than zero (Fig. 4G; DS = 1.91 ± 0.72 , port entry = 2.10 ± 0.94 , lick = 1.90 ± 0.66 ; all p values < 0.05). Therefore, all three task events (cue onset, reward seeking, and consumption) are contributing to the VP GABA calcium response.

VP GABA cue response predicts motivational value of the reward-predictive cue

We next sought to determine whether DS cue-evoked VP GABA calcium activity is correlated with port entry latency on a trial-by-trial basis. Previous work found that the DS-evoked spiking activity of many single units in VP is predictive of the latency it takes the animal to perform the behavior needed to obtain reward, whether that behavior is a lever press or a port entry (Richard et al., 2016, 2018). Because the encoding model described above revealed significant port-entry-related increases in calcium activity after, but not before, port entry, for our correlation analysis we only used calcium signals between cue onset and the port entry to examine how cue-elicited VP GABA activity predicted the latency of the animal to enter the port. Latency correlations were calculated for each rat individually in 0.10 s time bins and compared with shuffled controls (Fig. 4H). When we examined the mean correlation coefficients over time, we found that post-DS VP GABA calcium activity is initially positively

correlated with port entry latency when compared with shuffled data in the 0–0.50 s time bins ($p < 0.006$). This ramping positive correlation is initiated pre cue onset, during the baseline period. This suggests that baseline activity may predict port entry latency, such that greater baseline VP GABA activity precue leads to a longer postcue latency to enter the port. However, the 1.10–1.20 s time bins after cue onset are negatively correlated to the latency to enter the port ($p < 0.03$). This significant time of negative correlation roughly aligns with kernel time bins in which we observed significant DS-evoked calcium activity (0.90–1.30 s bins). This suggests that VP GABA calcium activity in response to DS cue onset is predictive of port entry latency, such that higher VP GABA calcium activity is associated with shorter port entry latencies, thus, greater encoding of the motivational value of the cue.

VP GABA neurons have a response post-reward-predictive cue even in the absence of reward

Because calcium imaging is a proxy for neural activity with slow kinetics, and VP neurons have been shown to encode relative reward value, as well as prediction errors (Ottenheimer et al., 2018, 2020a), we next aimed to further dissect the nature of the VP GABA neuron calcium activity we observed in response to the port entry and initial lick epochs. First, we introduced a 1 s delay between port entry and reward delivery to further separate the timing of reward seeking and initial reward consumption. We also included probe trials where the reward-predictive cue was presented, but reward delivery did not occur after port entry (Fig. 5A). This allowed us to determine whether calcium activity is elevated postport entry even in the absence of reward, thus allowing us to see whether the port entry responses are related to reward consumption or evaluation. Rats were tested for 2 d in sessions in which 50% of DS trials were probe trials to prevent behavioral extinction. Reward-seeking behavior persisted through both probe days, where the DS port entry probability remained above our response criteria (port entry behavior during at least 70% of DS trials; Fig. 5B). Average VP GABA calcium traces during trials where reward was delivered at a 1 s delay had two distinct peaks, suggesting that the port entry response was delayed somewhat to match the new reward timing (Fig. 5C). Interestingly, this VP GABA response was present even on probe trials, where no reward was delivered. Comparison of the AUC of VP GABA response between the rewarded trials and probe trials revealed no significant difference between the two signals (Fig. 5D; rewarded, 5.38 ± 0.92 ; probe, 6.38 ± 0.73 ; $F_{(1,33,99)} = 0.10$, $p = 0.75$; Bayes factor of 4.17 in favor of the null). Therefore, VP GABA neurons still respond to the cue and at the time that reward delivery is expected in the absence of reward. This suggests that VP GABA calcium activity responses after the port entry may be more related to reward anticipation or expectation than to actual reward consumption or evaluation.

VP GABA neuronal response decreases with extinction of learned behavior

Finally, we examined how consistent omission of reward affected reward-seeking behavior and VP GABA calcium activity. Rats received extinction training for 3 d immediately after probe trial days, where the DS was played, but no reward was delivered after port entry. The DS port entry probability of the rats decreased significantly across extinction training days (Fig. 6A; main effect of day, $F_{(2,17)} = 16.85$, $p < 0.002$). VP GABA calcium activity followed a similar pattern, where higher calcium activity in response to the DS cue is seen on day 1 of extinction compared with days 2 and 3 of extinction (Fig. 6B). Analysis of the AUC of the traces found a trend toward a significant decrease across extinction days (Fig. 6C; main effect of day effect, $F_{(2,18)} = 2.77$, $p = 0.10$), and planned follow-up comparisons reveal that VP GABA activity on day 2 of extinction training was significantly reduced relative to day 1 (Fig. 6D; $p < 0.05$). This indicates that

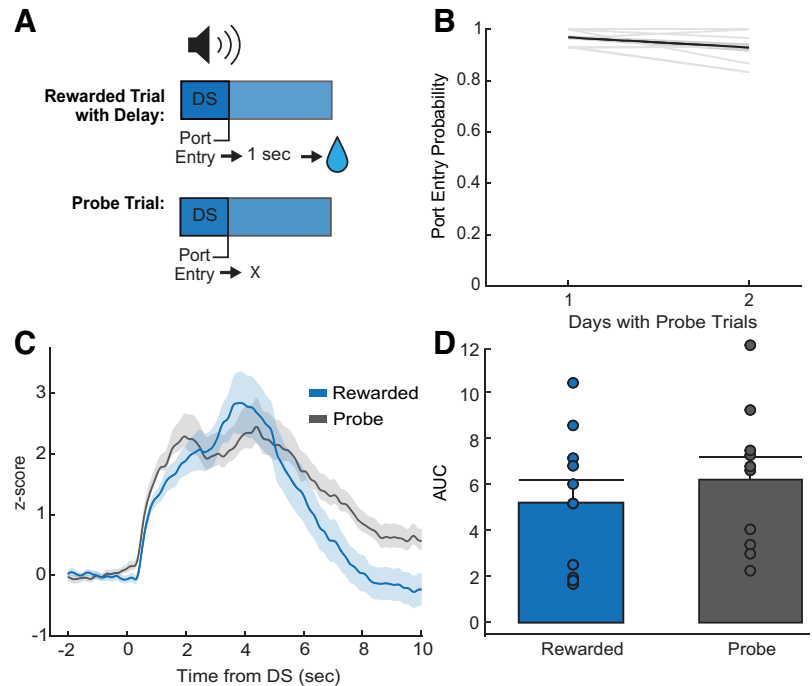


Figure 5. Effects of reward delivery and omission on DS calcium activity. **A**, Diagram of delayed reward DS trials and probe DS trials. **B**, Average DS port entry probability ($n = 10$ rats) across delayed reward and probe trial sessions (2 d). Behavior remains above criteria of 0.70. **C**, Average Z-score peri-DS calcium traces of delayed reward trials and probe trials averaged across animals ($n = 10$) for both days (blue, delayed reward trials; black, probe trials; \pm SEM). **D**, Average AUC of post-DS calcium traces (0–5 s) for delayed reward (blue) and probe trials (black) across animals ($n = 10$; \pm SEM). We observed no significant difference (sucrose, 5.38 ± 0.92 ; probe, 6.38 ± 0.73 ; $p = 0.78$; Bayes factor of 4.17 in favor of the null). Mean \pm SEM. Dots indicate individual subjects.

VP GABA calcium activity is sensitive to extinction learning and changes in the learned value of reward-predictive cues and cue-elicited reward seeking. Interestingly, both DS-elicited behavior and calcium activity remained above zero, potentially indicating some persistent motivational value of the cue, even after 3 d of extinction.

Optogenetic inhibition of VP GABA neurons reduces the probability and increases the latency of port entries during the DS

To assess the functional contribution of pericue VP GABA neuron activity, a separate group of rats ($n = 13$; 7 male, 6 female) were trained in the DS task, similarly to rats used for fiber photometry recordings (Fig. 7D). Rats were tested after reaching behavioral criteria in the DS task (Fig. 7E–H; laser duration, 0 s). On test days, rats received photoillumination of the VP (473 nm, 9–15 mW) on 50% of DS and NS trials, thus inhibiting VP GABA neurons in stGtACR animals ($n = 8$; 5 male, 3 female). Photoillumination was initiated at the start of the cue and terminated after 1 s on test day 1 and coterminated with the DS (after port entry or after 10 s, whichever occurred first) on test day 2 (Fig. 7D). We calculated the port entry probability (Fig. 7E,F) and port entry latency (Fig. 7G,H) for each trial type (laser off or laser on for DS and NS cues) in each animal. First, we examined impacts of optogenetic manipulations on reward-seeking behavior during the full 10 s cue period. We found that effects of brief 1 s laser delivery selectively increased the likelihood of responding to the NS (Fig. 7E; main effect of laser, $F_{(1,21)} = 2.74$, $p = 0.11$; laser by cue interaction, $F_{(1,21)} = 6.17$, $p = 0.021$) and decreased NS response latency (Fig. 7G; main effect of laser, $F_{(1,21)} = 1.17$, $p = 0.29$; laser by cue interaction, $F_{(1,21)} = 7.31$, $p = 0.13$). The

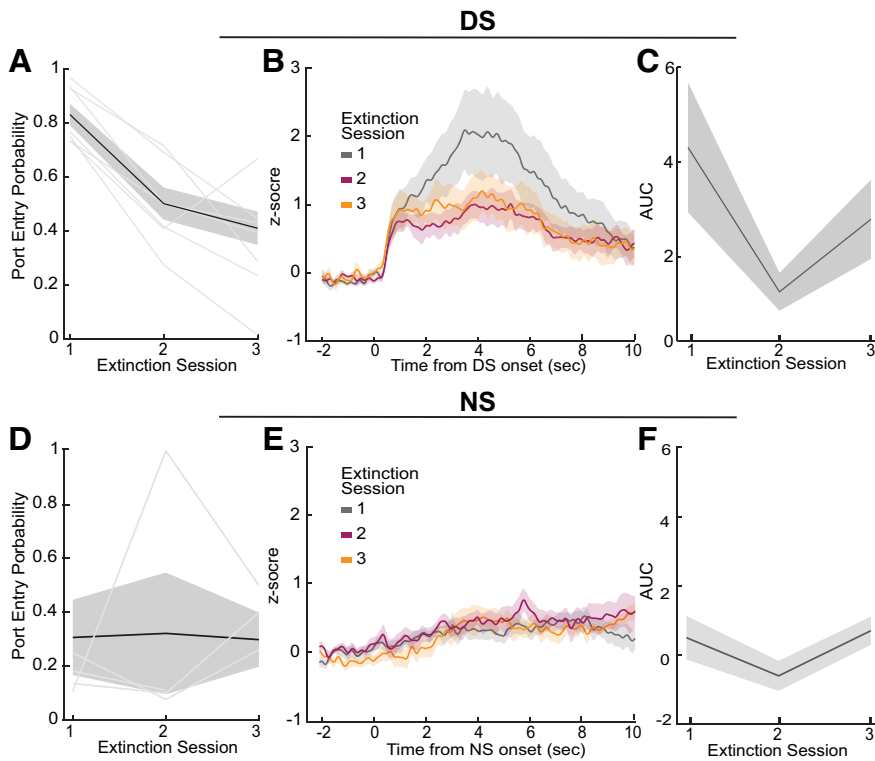


Figure 6. DS calcium activity during extinction learning. **A**, Average DS port entry probability across animals ($n = 8$) across extinction sessions (main effect of day, $F_{(2,17)} = 16.85$, $p < 0.002$). **B**, Average VP GABA calcium traces across animals ($n = 8$) for each day of training (\pm SEM). **C**, Average AUC of post-DS calcium traces (0–5 s) across animals ($n = 8$) for each session of extinction training (main effect of day, $F_{(2,18)} = 2.77$, $p = 0.11$). **D**, Average NS port entry probability across animals across extinction sessions. **E**, Average VP NS GABA calcium traces across animals for each day of training. **F**, Average AUC of post-NS calcium traces across animals for each session of extinction training. Lines with shading indicate mean \pm SEM. Lines alone indicate individual subjects.

same effects were not seen in control animals (Fig. 7F; main effect of laser, $F_{(1,12)} = 0.32$, $p = 0.58$; laser by cue interaction, $F_{(1,12)} = 0.19$, $p = 0.67$) or port entry latency (Fig. 7G; main effect of laser, $F_{(1,12)} = 0.18$, $p = 0.68$; laser by cue interaction, $F_{(1,12)} = 0.19$, $p = 0.67$). In contrast, inhibition of VP GABA neurons for the full length of the cue significantly decreased port entry probability during the DS but not the NS (Fig. 7D; main effect of laser, $F_{(1,21)} = 7.83$, $p = 0.01$; laser by cue interaction, $F_{(1,21)} = 12.0$, $p = 0.002$) and significantly increased port entry latency for the DS but not the NS (Fig. 7E; main effect of laser, $F_{(1,21)} = 10.53$, $p = 0.004$; laser by cue interaction, $F_{(1,21)} = 13.75$, $p = 0.001$). The same effects were not seen in control animals ($n = 5$; 2 male, 3 female) for either port entry probability (Fig. 7F; main effect of laser, $F_{(1,16)} = 0.0083$, $p = 0.93$; laser by cue interaction, $F_{(1,16)} = 0.0083$, $p = 0.93$) or port entry latency (Fig. 7G; main effect of laser, $F_{(1,16)} = 0.17$, $p = 0.69$; laser by cue interaction, $F_{(1,16)} = 0.23$, $p = 0.64$).

Although brief inhibition did not have an impact on behavior during the DS when averaged across the whole 10 s cue period, we wanted to further dissect behavior during and shortly after the inhibition period. To do this we first calculated the cumulative proportion of trials occurring at each response latency across animals for each trial type (Fig. 7H,I). This revealed a rightward shift in the distribution of latencies during the DS trials paired with 1 s inhibition of VP GABA neurons. Follow-up analyses revealed that 1 s inhibition of VP GABA neurons significantly decreased DS port entry probability within 1 s of cue onset (Fig. 7H; main effect of laser, $F_{(1,21)} = 7.57$, $p = 0.01$; laser by cue

interaction, $F_{(1,21)} = 11.60$, $p = 0.003$; laser vs no laser DS trials, $t_{(21)} = 4.354$, $p = 0.0003$). Although 1 s inhibition increased NS response probability during the full 10 s cue period, this did not occur during the 1 s inhibition itself (laser vs no laser NS trials, $t_{(21)} = -0.462$, $p = 0.649$). Instead, the probability of NS responses appears to selectively increase after inhibition offset (Fig. 7I), perhaps because of rebound excitation of VP GABA neurons (Mahn et al., 2018; Messier et al., 2018; Hughes et al., 2020).

Discussion

We assessed population-level calcium activity in VP GABA neurons while rats learned and performed a cue-elicited reward-seeking task. As rats learned, calcium responses developed to the reward-predictive cue but not the neutral cue. An encoding model revealed encoding of the reward-predictive cue, as well as the operant behavior and initial reward consumption. These responses were similar in magnitude and occurred after, but not before, event onsets. Calcium activity evoked by the reward-predictive cue also predicted the latency of reward-seeking behavior. Additionally, VP GABA inhibition during reward cue presentation decreased reward-seeking probability and increased the latency of reward-seeking behavior. Neuronal responses to the cues and operant behavior persisted even

on trials with reward omission. However, when reward was completely omitted from all trials, behavior of the rats, and calcium responses to the reward-predictive cue, decreased. These findings support the hypothesis that VP GABA neurons encode reward-seeking motivation and vigor.

Ventral pallidal GABA neurons develop calcium responses to cues across learning

Consistent with our overall hypothesis, we observed increased VP GABA calcium activity selectively in response to a cue-predicting reward availability. Increased firing by these neurons to reward-paired cues has previously been observed in a pavlovian paradigm (Stephenson-Jones et al., 2020). Specifically, spiking activity of optogenetically identified VP GABA neurons is elevated in response to a cue-predicting water reward in thirsty mice. Additionally, cue-evoked excitatory responses are blunted as mice become satiated on water. These findings suggest that VP GABA neurons may encode the motivational value of cues, but it remained unclear whether this would extend to instrumental reward seeking in freely moving rats or to trial-by-trial variations in motivated behavior that are independent of gradual changes in learned cue value because of satiation. Additionally, we wanted to assess the development of these responses across training.

Previous work using *in vivo* electrophysiology to record VP units in a non-cell-type-specific manner found excitatory responses to rewards and reward-related cues in both

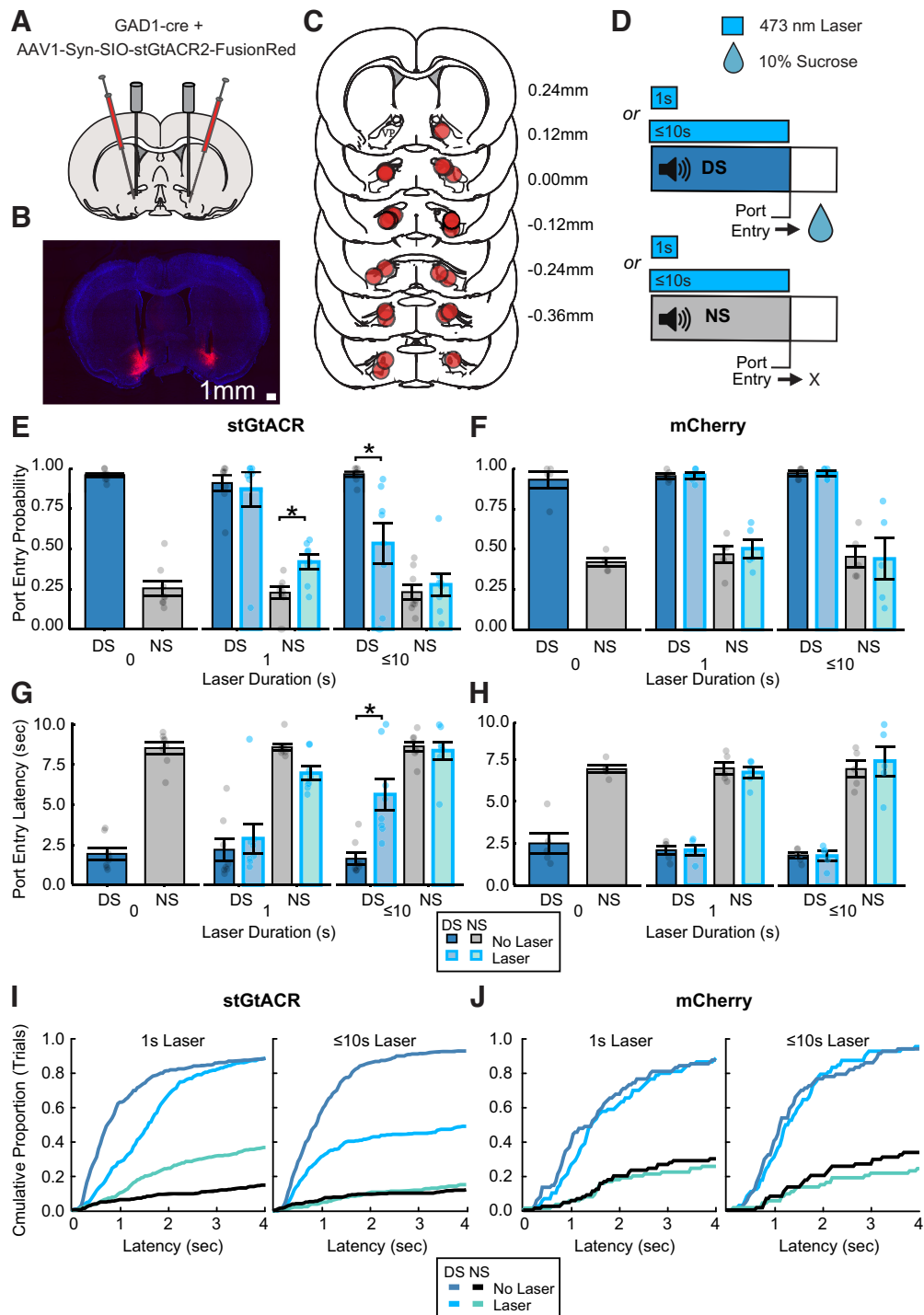


Figure 7. Optogenetic inhibition of VP GABA during cue presentation. **A**, Injection and fiber implant paradigm for targeting StGtACR2 to VP GABA neurons. **B**, Representative VP section with bilateral mCherry expression and fiber implant tracts. **C**, Fiber implant locations of stGtACR inhibition ($n = 8$) and mCherry control ($n = 5$) animals. **D**, DS task optogenetic test day trial design with continuous 473 nm laser on 50% of trials of each cue type. **E**, Port entry probability of stGtACR animals ($n = 8$) on the day before laser tests (laser duration, 0), 1 s laser test day, and up to 10 s laser test day, during DS trials with no laser (blue with black outline), DS trials with laser (light blue with cyan outline), NS trials with no laser (gray with black outline), and NS trials with laser (sea green with cyan outline). Data are represented as mean \pm SEM. Dots represent individual rats. For pairwise follow-up comparisons, $*p < 0.05$. **F**, Average DS and NS port entry probability of control animals with and without laser ($n = 5$). **G**, Average DS and NS port entry latency of stGtACR animals with and without laser. **H**, Average DS and NS port entry latency of control animals with and without laser. **I**, Cumulative distribution plots of port entry latency in stGtACR animals for DS trials with no laser (medium blue), DS trials with laser (cyan), NS trials with no laser (black), and NS trials with laser (sea green) during sessions with 1 s inhibition (left) or up to 10 s inhibition (right). **J**, Cumulative distribution plots of control animals.

pavlovian and instrumental paradigms (Tindell et al., 2004, 2005; Smith et al., 2009, 2011; Ahrens et al., 2016; Richard et al., 2016; Ottenheimer et al., 2018, 2020a). In a pavlovian paradigm, the proportion of VP neurons excited by a reward-paired cue increases from early to late training as

behavioral responses to the cue develop (Tindell et al., 2004). To our knowledge, the development of VP cue responses over time has not previously been reported in an instrumental setting. Here, cue-evoked calcium activity increased as rats learned the DS task. Our population-

level measurements make it unclear whether this is because of rate or population level encoding but are consistent with VP encoding of learned cue value in an instrumental task.

Importantly, the observed pericue calcium response persisted for multiple seconds after cue onset. The kinetics of even the relatively fast GCaMP6f calcium sensor used here limit our ability to separate out responses to individual behavioral events, especially when assessing responses averaged across trials. To more accurately isolate responses to specific behavioral events, and to determine whether peri-DS calcium activity is attributable to the DS specifically, we used linear regression to evaluate how associated each behavioral epoch was with the calcium signal at each time point of the task (Parker et al., 2016). With this encoding model, we demonstrate that VP GABA calcium activity encodes the reward-predictive cue. This is consistent with previous work showing increases in VP spiking activity immediately after cue onset in instrumental and pavlovian paradigms (Tindell et al., 2004; Richard et al., 2016, 2018; Ottenheimer et al., 2018, 2020a; Stephenson-Jones et al., 2020).

Encoding of reward-seeking latency by VP GABA cue-evoked activity

We also demonstrate that although precue VP GABA calcium activity is positively correlated with trial-by-trial latency, this relationship switches to a negative correlation around the time of DS-evoked calcium activity. This negative correlation suggests that greater DS-evoked VP GABA calcium activity predicts reward-seeking latency or vigor. Prior work using *in vivo* electrophysiology has also reported a negative correlation between DS-evoked activity and reward-seeking latency (Richard et al., 2016, 2018), as well as a positive relationship with other behavioral measures of cue-evoked motivation, including the speed of the upcoming approach movement and the proximity of the animal to the movement target at cue onset (Lederman et al., 2021). About 20–25% of neurons are reported to have significant negative correlations between postcue firing and reward-seeking latency; our findings suggest that at least some of these neurons are GABAergic. Additionally, optogenetic inhibition of VP GABA neurons during reward cue presentation decreases port entry probability and increases port entry latency. Importantly, even brief 1 s inhibition of VP GABA neurons at cue onset was sufficient to shift the distribution of DS response latencies, reducing the probability of reward-seeking responses during the first second of cue onset. Although DS responses recovered, and NS responses increased over no laser conditions after inhibition offset, this may be due in part to rebound excitation of VP GABA neurons (Mahn et al., 2018; Messier et al., 2018; Hughes et al., 2020). Overall, this functional manipulation is further evidence that VP GABA neurons promote reward-seeking motivation and vigor. The positive correlation between precue (and early postcue) VP GABA activity and trial-by-trial latency reported here was unexpected as it has not been reported in prior work using electrophysiology, at least on average across VP single units. Whether this correlation is related to our cell-type-specific approach or to calcium activity specifically is an open question.

Elevation of calcium activity following port entry and during initial reward consumption

The encoding model revealed that VP GABA neuron calcium activity is also evoked following the operant behavior (port entry)

required to obtain the sucrose reward. This is consistent with prior work (Richard et al., 2016) showing that VP single units are excited at both the time of an operant response (lever press) and at entry into the reward port. To better assess the influence of the reward-seeking action versus reward expectation or evaluation, we added a delay between port entry and reward delivery as well as DS probe trials where no reward was delivered following port entry. When the timing of reward delivery after port entry is delayed, the timing of the calcium activity shifts to match. This suggests that it is not an action-related response but either a reward expectation or evaluation. When we separated reward trials from probe trials, we observed very similar calcium responses in neurons no matter the trial type, suggesting that the calcium response is more related to expectation than reward evaluation or hedonic impact.

Finally, the encoding model showed that part of the calcium response was associated with the first lick after rewarded port entry (i.e., the beginning of sucrose consumption). This is consistent with prior work showing that VP GABA neurons respond to reward delivery (Stephenson-Jones et al., 2020) and are implicated in consumption of palatable reward in sated animals (Farrell et al., 2021). However, VP GABA activity was also observed on probe trials where no sucrose was delivered. This suggests that VP GABA calcium activity associated with the initial lick is encoding expectancy of reward that is independent of the presence or value of reward once rats learn the behavioral paradigm. This differs from previous work showing that a subset of VP neurons, most likely including VP GABA neurons, is sensitive to reward identity and encode reward value (Ottenheimer et al., 2020a; Stephenson-Jones et al., 2020).

Caveats and future directions

Here, we used population-level calcium imaging to examine encoding of behavioral events. Although the time scale of neuronal activation is captured more accurately with electrophysiological recordings, cell-type-specific recording is easier to achieve with calcium imaging approaches, as is measurement of activity from neurons with low basal firing rates (Wei et al., 2020). We found that VP GABA calcium activity increases in response to a reward-predictive cue and at the time of expected reward consumption. Unexpectedly, we found that the calcium response at the time of expected reward delivery was insensitive to reward omission. This is surprising because of the finding that VP neurons are sensitive to the relative reward value and can encode reward-prediction errors (Ottenheimer et al., 2020a). This discrepancy could be in part because of limitations of bulk calcium imaging. Recent work suggests that fiber photometry recordings of calcium activity may be more indicative of nonsomatic activity, representing inputs to neurons as opposed to outputs of the neurons (Legaria et al., 2022). We may be capturing dendritic calcium changes, which may not reflect the same electrophysiological responses that encode relative reward value or reward-prediction error signals. We can also not fully rule out potential contributions of axonal signals from nearby GABAergic inputs to VP, although we observed no-to-minimal cell body expression in adjacent structures (data not shown). Future work could examine soma-specific calcium activity in the DS task using soma-targeted viral expression and/or miniscope imaging (Aharoni and Hoogland, 2019; Chen et al., 2020; Shemesh et al., 2020). Our finding that calcium activity persists even when reward is omitted could also be because of heterogeneity in the response patterns of VP GABA neurons. Importantly, signals

encoding relative reward value and reward-prediction error-like signals have just been observed in subsets of VP neurons (Ottenheimer et al., 2018, 2020a,b). VP GABA neurons may differ in their encoding and functional contributions based on more specific cell-type subdivisions or output pathways. For instance, some work points to parvalbumin neurons being a subset of VP GABA neurons involved in cue-evoked behaviors (Prasad et al., 2020), whereas Npas1-positive VP GABA neurons may contribute to stress and anxiety-related behaviors (Morais-Silva et al., 2022). Additionally, VP GABA neurons have many projection targets that have varied roles in appetitive behavior (Covelo et al., 2014; Mahler et al., 2014; Leung and Balleine, 2015; Root et al., 2015; Prasad and McNally, 2016; Farrell et al., 2021; Vachez et al., 2021; Morais-Silva et al., 2022). Probing a more specific subset of VP GABA cells (cell type or projection specific) may reveal greater, or a lack of, encoding of cue-elicited reward seeking and reward evaluation.

References

- Aharoni D, Hoogland TM (2019) Circuit investigations with open-source miniaturized microscopes: past, present and future. *Front Cell Neurosci* 13:141.
- Ahrens AM, Meyer PJ, Ferguson LM, Robinson TE, Aldridge JW (2016) Neural activity in the ventral pallidum encodes variation in the incentive value of a reward cue. *J Neurosci* 36:7957–7970.
- Buck SA, et al. (2021) Vesicular glutamate transporter modulates sex differences in dopamine neuron vulnerability to age-related neurodegeneration. *Aging Cell* 20:e13365.
- Chen T-W, Wardill TJ, Sun Y, Pulver SR, Renninger SL, Baohan A, Schreier ER, Kerr RA, Orger MB, Jayaraman V, Looger LL, Svoboda K, Kim DS (2013) Ultrasensitive fluorescent proteins for imaging neuronal activity. *Nature* 499:295–300.
- Chen Y, Jang H, Spratt PWE, Kosar S, Taylor DE, Essner RA, Bai L, Leib DE, Kuo T-W, Lin Y-C, Patel M, Subkhangulova A, Kato S, Feinberg EH, Bender KJ, Knight ZA, Garrison JL (2020) Soma-targeted imaging of neural circuits by ribosome tethering. *Neuron* 107:454–469.e6.
- Covelo IR, Patel ZI, Luviano JA, Stratford TR, Wirtshafter D (2014) Manipulation of GABA in the ventral pallidum, but not the nucleus accumbens, induces intense, preferential, fat consumption in rats. *Behav Brain Res* 270:316–325.
- Dana H, Novak O, Guardado-Montesino M, Fransen JW, Hu A, Borghuis BG, Guo C, Kim DS, Svoboda K (2018) Thy1 transgenic mice expressing the red fluorescent calcium indicator jRGECO1a for neuronal population imaging *in vivo*. *PLoS One* 13:e0205444.
- Faget L, Zell V, Souter E, McPherson A, Ressler R, Gutierrez-Reed N, Yoo JH, Dulcis D, Hnasko TS (2018) Opponent control of behavioral reinforcement by inhibitory and excitatory projections from the ventral pallidum. *Nat Commun* 9:849.
- Farrell MR, Esteban JSD, Faget L, Floresco SB, Hnasko TS, Mahler SV (2021) Ventral pallidum GABA neurons mediate motivation underlying risky choice. *J Neurosci* 41:4500–4513.
- Farrell MR, Ye Q, Xie Y, Esteban JSD, Mahler SV (2022) Ventral pallidum GABA neurons bidirectionally control opioid relapse across rat behavioral models. *Addict Neurosci* 3:100026.
- Fries-Craft KA, Meyer MM, Lindblom SC, Kerr BJ, Bobeck EA (2021) Lipid source and peroxidation status alter immune cell recruitment in broiler chicken ileum. *J Nutr* 151:223–234.
- Giannini LAA, Peterson C, Ohm D, Xie SX, McMillan CT, Raskovsky K, Massimo L, Suh E, Van Deerlin VM, Wolk DA, Trojanowski JQ, Lee EB, Grossman M, Irwin DJ (2021) Frontotemporal lobar degeneration protei-nopathies have disparate microscopic patterns of white and grey matter pathology. *Acta Neuropathol Commun* 9:30.
- Gómez-A A, Shnitko TA, Caref KL, Nicola SM, Robinson DL (2022) Stimuli predicting high-calorie reward increase dopamine release and drive approach to food in the absence of homeostatic need. *Nutr Neurosci* 25:593–602.
- He Z, McBride JD, Xu H, Changolkar L, Kim S, Zhang B, Narasimhan S, Gibbons GS, Guo JL, Kozak M, Schellenberg GD, Trojanowski JQ, Lee VM-Y (2020) Transmission of tauopathy strains is independent of their isoform composition. *Nat Commun* 11:7.
- Heinsbroek JA, Bobadilla A-C, Dereschewitz E, Assali A, Chalhoub RM, Cowan CW, Kalivas PW (2020) Opposing regulation of cocaine seeking by glutamate and GABA neurons in the ventral pallidum. *Cell Rep* 30:2018–2027.e3.
- Hughes RN, Bakhurin KI, Petter EA, Watson GDR, Kim N, Friedman AD, Yin HH (2020) Ventral tegmental dopamine neurons control the impulse vector during motivated behavior. *Curr Biol CB* 30:2681–2694.e5.
- Kupchik YM, Prasad AA (2021) Ventral pallidum cellular and pathway specificity in drug seeking. *Neurosci Biobehav Rev* 131:373–386.
- Lederman J, Lardeux S, Nicola SM (2021) Vigor encoding in the ventral pallidum. *eNeuro* 8:ENEURO.0064-21.2021.
- Legaria AA, Matikainen-Ankney BA, Yang B, Ahanonu B, Licholai JA, Parker JG, Kravitz AV (2022) Fiber photometry in striatum reflects primarily nonsomatic changes in calcium. *Nat Neurosci* 25:1124–1128.
- Leung BK, Balleine BW (2015) Ventral pallidal projections to mediodorsal thalamus and ventral tegmental area play distinct roles in outcome-specific Pavlovian-instrumental transfer. *J Neurosci* 35:4953–4964.
- Liu Y-J, Ehrenguber MU, Negwer M, Shao H-J, Cetin AH, Lyon DC (2013) Tracing inputs to inhibitory or excitatory neurons of mouse and cat visual cortex with a targeted rabies virus. *Curr Biol* 23:1746–1755.
- Mahler SV, Vazey EM, Beckley JT, Keistler CR, McGlinchey EM, Kaufling J, Wilson SP, Deisseroth K, Woodward JJ, Aston-Jones G (2014) Designer receptors show role for ventral pallidum input to ventral tegmental area in cocaine seeking. *Nat Neurosci* 17:577–585.
- Mahn M, Gibor L, Patil P, Cohen-Kashi Malina K, Oring S, Printz Y, Levy R, Lampl I, Yizhar O (2018) High-efficiency optogenetic silencing with soma-targeted anion-conducting channelrhodopsins. *Nat Commun* 9:4125.
- McMillan P, Wheeler J, Gatlin RE, Taylor L, Strovos T, Baum M, Bird TD, Latimer C, Keene CD, Kraemer BC, Liachko NF (2020) Adult onset pan-neuronal human tau tubulin kinase 1 expression causes severe cerebellar neurodegeneration in mice. *Acta Neuropathol Commun* 8:200.
- Meng C, Zhou J, Papaneri A, Peddada T, Xu K, Cui G (2018) Spectrally resolved fiber photometry for multi-component analysis of brain circuits. *Neuron* 98:707–717.e4.
- Messier JE, Chen H, Cai Z-L, Xue M (2018) Targeting light-gated chloride channels to neuronal somatodendritic domain reduces their excitatory effect in the axon. *Elife* 7:e38506.
- Morais-Silva G, Campbell RR, Nam H, Basu M, Pagliusi M, Fox ME, Chan S, Iniguez SD, Ament S, Cramer N, Marin MT, Lobo MK (2022) Molecular, circuit, and stress response characterization of ventral pallidum Npas1-neurons. *J Neurosci* 43:405–418.
- Ottenheimer D, Richard JM, Janak PH (2018) Ventral pallidum encodes relative reward value earlier and more robustly than nucleus accumbens. *Nat Commun* 9:4350.
- Ottenheimer DJ, Bari BA, Sutlief E, Fraser KM, Kim TH, Richard JM, Cohen JY, Janak PH (2020a) A quantitative reward prediction error signal in the ventral pallidum. *Nat Neurosci* 23:1267–1276.
- Ottenheimer DJ, Wang K, Tong X, Fraser KM, Richard JM, Janak PH (2020b) Reward activity in ventral pallidum tracks satiety-sensitive preference and drives choice behavior. *Sci Adv* 6:eabc9321.
- Parker NF, Cameron CM, Taliaferro JP, Lee J, Choi JY, Davidson TJ, Daw ND, Witten IB (2016) Reward and choice encoding in terminals of mid-brain dopamine neurons depends on striatal target. *Nat Neurosci* 19:845–854.
- Patel JM, Swanson J, Ung K, Herman A, Hanson E, Ortiz-Guzman J, Selever J, Tong Q, Arenkiel BR (2019) Sensory perception drives food avoidance through excitatory basal forebrain circuits. *Elife* 8:e44548.
- Prasad AA, McNally GP (2016) Ventral pallidum output pathways in context-induced reinstatement of alcohol seeking. *J Neurosci* 36:11716–11726.
- Prasad AA, Xie C, Chaichim C, Nguyen JH, McClusky HE, Killcross S, Power JM, McNally GP (2020) Complementary roles for ventral pallidum cell types and their projections in relapse. *J Neurosci* 40:880–893.
- Richard JM, Ambroggi F, Janak PH, Fields HL (2016) Ventral pallidum neurons encode incentive value and promote cue-elicited instrumental actions. *Neuron* 90:1165–1173.
- Richard JM, Stout N, Acs D, Janak PH (2018) Ventral pallidal encoding of reward-seeking behavior depends on the underlying associative structure. *Elife* 7:e33107.

- Root DH, Melendez RI, Zaborszky L, Napier TC (2015) The ventral pallidum: subregion-specific functional anatomy and roles in motivated behaviors. *Prog Neurobiol* 130:29–70.
- Saunders BT, Richard JM, Margolis EB, Janak PH (2018) Dopamine neurons create Pavlovian conditioned stimuli with circuit-defined motivational properties. *Nat Neurosci* 21:1072–1083.
- Shahidehpour RK, Higdon RE, Crawford NG, Neltner JH, Ighodaro ET, Patel E, Price D, Nelson PT, Bachstetter AD (2021) Dystrophic microglia are associated with neurodegenerative disease and not healthy aging in the human brain. *Neurobiol Aging* 99:19–27.
- Shemesh OA, et al. (2020) Precision calcium imaging of dense neural populations via a cell-body-targeted calcium indicator. *Neuron* 107:470–486.e11.
- Shields AK, Suarez M, Wakabayashi KT, Bass CE (2021) Activation of VTA GABA neurons disrupts reward seeking by altering temporal processing. *Behav Brain Res* 410:113292.
- Smith KS, Tindell AJ, Aldridge JW, Berridge KC (2009) Ventral pallidum roles in reward and motivation. *Behav Brain Res* 196:155–167.
- Smith KS, Berridge KC, Aldridge JW (2011) Disentangling pleasure from incentive salience and learning signals in brain reward circuitry. *Proc Natl Acad Sci U S A* 108:E255–E264.
- Stephenson-Jones M, Bravo-Rivera C, Ahrens S, Furlan A, Xiao X, Fernandes-Henriques C, Li B (2020) Opposing contributions of GABAergic and glutamatergic ventral pallidal neurons to motivational behaviors. *Neuron* 105:921–933.e5.
- Tian L, Hires SA, Mao T, Huber D, Chiappe ME, Chalasani SH, Petreanu L, Akerboom J, McKinney SA, Schreiter ER, Bargmann CI, Jayaraman V, Svoboda K, Looger LL (2009) Imaging neural activity in worms, flies and mice with improved GCaMP calcium indicators. *Nat Methods* 6:875–881.
- Tindell AJ, Berridge KC, Aldridge JW (2004) Ventral pallidal representation of pavlovian cues and reward: population and rate codes. *J Neurosci* 24:1058–1069.
- Tindell AJ, Berridge KC, Zhang J, Peciña S, Aldridge JW (2005) Ventral pallidal neurons code incentive motivation: amplification by meso-limbic sensitization and amphetamine. *Eur J Neurosci* 22:2617–2634.
- Tooley J, Marconi L, Alipio JB, Matikainen-Ankney B, Georgiou P, Kravitz AV, Creed MC (2018) Glutamatergic ventral pallidal neurons modulate activity of the habenula–tegmental circuitry and constrain reward seeking. *Biol Psychiatry* 83:1012–1023.
- Vachez YM, Tooley JR, Abiraman K, Matikainen-Ankney B, Casey E, Earnest T, Ramos LM, Silberberg H, Godynnyuk E, Uddin O, Marconi L, Le Pichon CE, Creed MC (2021) Ventral arkypallidal neurons inhibit accumbal firing to promote reward consumption. *Nat Neurosci* 24:379–390.
- Verbeke G (1997) Linear mixed models for longitudinal data. In: *Linear mixed models in practice: an SAS-oriented approach* (Verbeke G, Molenberghs G, eds), pp 63–153. New York: Springer.
- Wakabayashi KT, Feja M, Baidur AN, Bruno MJ, Bhimani RV, Park J, Hausknecht K, Shen R-Y, Haj-Dahmane S, Bass CE (2019) Chemogenetic activation of ventral tegmental area GABA neurons, but not mesoaccumbal GABA terminals, disrupts responding to reward-predictive cues. *Neuropsychopharmacology* 44:372–380.
- Wei Z, Lin B-J, Chen T-W, Daie K, Svoboda K, Druckmann S (2020) A comparison of neuronal population dynamics measured with calcium imaging and electrophysiology. *PLoS Comput Biol* 16:e1008198.